Photocatalytic Degradation of the Antibiotic Sulfamethazine Using Decatungstate Anions in an Aqueous Solution: Mechanistic Approach

Mohammed-Amine Edaala, Lekbira El Mersly, Abdelaziz Aloui Tahiri, Pascal Wong-Wah-Chung, Lahssen El Blidi, Maher M Alrashed, Salah Rafqah

water

MDPI

Article

Photocatalytic Degradation of the Antibiotic Sulfamethazine Using Decatungstate Anions in an Aqueous Solution: Mechanistic Approach

Mohammed-Amine Edaala [1,*], Lekbira El Mersly [1], Abdelaziz Aloui Tahiri [1], Pascal Wong-Wah-Chung [2], Lahssen El Blidi [3], Maher M. Alrashed [3] and Salah Rafqah [1]

[1] Laboratoire de Chimie Analytique et Moléculaire, Faculté Polydisciplinaire de Safi, Université Cadi Ayyad, Sidi Bouzid, B.P. 4162, Safi 46000, Morocco; lekbira.elmersly@ced.uca.ma (L.E.M.); az_alaoui@yahoo.fr (A.A.T.); s.rafqah@uca.ma (S.R.)

[2] Aix Marseille Université, CNRS, LCE, Bâtiment Villemin BP 80, 13545 Aix-en-Provence Cedex 4, France; pascal.wong-wah-chung@univ-amu.fr

[3] Chemical Engineering Department, College of Engineering, King Saud University, P.O. Box 800, Riyadh 11421, Saudi Arabia; lelblidi@ksu.edu.sa (L.E.B.); mabdulaziz@ksu.edu.sa (M.M.A.)

* Correspondence: m.edaala.ced@uca.ac.ma; Tel.: +212-651-345751

Abstract: The aim of this study is to propose a successful method for the treatment of water contaminated by pharmaceutical pollutants through homogeneous photocatalysis in the presence of decatungstate ions ($W_{10}O_{32}^{4-}$). Sulfamethazine (SMZ), a sulfonamide antibiotic, was used as a model molecule. The results showed that SMZ could be effectively degraded with this process under simulated solar irradiation. SMZ degradation kinetics were studied with different dioxygen and SMZ concentrations, pH values, and photocatalyst masses. Optimal conditions were determined to be pH 7, $[Na_4W_{10}O_{32}]$ = 0.33 g/L, and [SMZ] = 13.9 mg/L under the aerated condition, resulting in 85% SMZ degradation in 240 min, using a 36W-UVA/UVB light source. Hydroxyl radicals were identified as the major contributors to SMZ elimination. Four photoproducts identified with high-performance liquid chromatography coupled with mass spectrometry were formed by the cleavage of the sulfonamide bond and the hydroxylation of both the aromatic ring and pyrimidine moiety. SMZ was completely mineralized after 90 h of irradiation in the presence of decatungstate anions. These results provided a mechanism for the photocatalytic degradation of SMZ in an aqueous solution. To sustain this mechanism, theoretical studies were carried out using density functional theory calculations. This involved Fukui functional analyses, including ring hydroxylation, C-S bond cleavage, and molecular rearrangement processes.

Keywords: decatungstate ions; antibiotic; photocatalysis; hydroxyl radicals; SMZ; mineralization

Citation: Edaala, M.-A.; El Mersly, L.; Aloui Tahiri, A.; Wong-Wah-Chung, P.; El Blidi, L.; Alrashed, M.M.; Rafqah, S. Photocatalytic Degradation of the Antibiotic Sulfamethazine Using Decatungstate Anions in an Aqueous Solution: Mechanistic Approach. *Water* **2023**, *15*, 4058. https://doi.org/10.3390/w15234058

Academic Editor: Alexandre T. Paulino

Received: 28 October 2023
Revised: 10 November 2023
Accepted: 17 November 2023
Published: 23 November 2023

1. Introduction

Thousands of tons of pharmaceuticals are produced and consumed annually to improve human and animal health. However, a significant portion of these enter the environment through various pathways, including human, industrial, and veterinary activities [1]. These substances are persistent pollutants and can be pharmacologically active and toxic [2,3]. Although the actual risks to humans are still unclear, some research indicates that they can damage the ecosystem and have dangerous effects on humans and wildlife [4,5].

Pharmaceutical compounds detected in wastewater are often classified as polar micropollutants that cannot be readily removed using conventional wastewater treatment plants (WWTPs) [6]. Sulfonamide antibiotics are widely used in the treatment of various bacterial infections due to their low cost, low toxicity, and high efficiency [7]. They have been detected in municipal WWTP effluents at concentrations ranging from 70 to

227 ng/L [8,9]. In surface waters, the occurrence of sulfonamides has been confirmed with concentrations in the range 21–132 ng/L in Japanese rivers and 0.1–42.5 ng/L in Spanish ones, supporting their partial removal during wastewater treatment [10,11].

In recent decades, many techniques have been employed for wastewater treatment. Chemical coagulation and precipitation stand out as efficient methods for removing pharmaceuticals from wastewater. These processes entail the formation of insoluble complexes, easily separable through sedimentation or filtration [12]. Another widely used approach involves activated carbon, which has demonstrated remarkable efficiency in adsorbing various organic compounds, including pharmaceutical residues, from wastewater [13]. Biological treatment methods, such as conventional activated sludge and aerobic bioreactors, can also be tailored for pharmaceutical wastewater treatment. Microorganisms play a pivotal role in biodegrading pharmaceutical compounds, albeit some may display resistance, necessitating longer hydraulic retention times for complete removal [14,15]. Furthermore, membrane-based technologies such as nano-filtration and reverse osmosis have proven valuable for eliminating both organic and inorganic contaminants, including pharmaceuticals, from wastewater [16].

Recently, numerous studies have focused on advanced oxidation processes for the removal of pharmaceutical pollutants from wastewaters [17–20]. These processes have demonstrated their effectiveness against toxic and non-biodegradable organic pollutants. In general, the excitation of the photoactive material under the action of artificial or natural light leads to the formation of hydroxyl radicals ($OH^{\bullet}$). These radicals are very strong oxidizing agents, i.e., they can oxidize many organic compounds, up to mineralization (conversion of the pollutants into CO_2, H_2O, and inorganic ions) [17,19–22].

In addition, polyoxometalates (POMs) are a model of a homogenous photocatalyst and have attracted much attention for their photocatalytic activities due to their charge transfer properties; the first report of these compounds in photochemistry was published over 100 years ago [23–27]. The decatungstate anion ($W_{10}O_{32}{}^{4-}$), a member of the POMs, has been shown to be one of the most active species for photocatalytic degradation of various organic pollutants with UV light [25,28–31]. The photoexcitation of the decatungstate anion occurs in the range of 300-400 nm, especially at the maximum absorption wavelength (λ_{max} = 324 nm). This leads to an excited state and the formation of photoexcited $W_{10}O_{32}{}^{4-*}$ through an intramolecular charge transfer from HOMO of O^{2-} to the LUMO of W^{6+}. The photoexcited radical is highly active and can act as an oxidant by electron transfer and/or as a reductant by hydrogen abstraction because it has an electron-deficient oxygen center. In addition, it can react with hydroxyl ions to form hydroxyl radicals responsible for the degradation of organic pollutants. Finally, the oxidized form of the decatungstate ion ($W_{10}O_{32}{}^{5-}$) reacts with dioxygen available in the medium to regenerate the initial form, allowing its reuse for photocatalytic applications [24,25].

This study aims to present an innovative method for treating water contaminated with pharmaceutical pollutants through the utilization of homogeneous photocatalysis in the presence of decatungstate ions. Homogeneous photocatalysis was selected due to its superior efficiency in degrading organic pollutants attributed to the direct interaction between the dissolved catalyst and pollutants, facilitating a less selective and more rapid and complete reaction [25,26,32,33]. Sulfamethazine (SMZ) is chosen as the model molecule due to its persistence in the aquatic environment, toxicity, and low photo and biodegradability [10,34]. The research will specifically focus on the process's efficiency under simulated solar irradiation (kinetics and mineralization) and the optimized conditions to achieve maximum SMZ degradation. In addition, the mechanistic pathways will be deeply explored by (i) investigating the short-lived species responsible for the degradation process, (ii) identifying the photoproducts, and (iii) carrying out theoretical studies using density functional theory calculations (DFT). The general goal is to emphasize the significance of this research in advancing environmental remediation strategies.

2. Materials and Methods

2.1. Materials

SMZ (MW of 279 g/mol) (99%) (Figure S1) and acetonitrile (HPLC grade) Isopropanol (IPA) (C_3H_7OH) (99.8%) CHROMANORM (Sigma Aldrich, Shanghai, China). Sodium tungstate (Na_2WO_4, $2H_2O$) and hydrochloric acid (HCl) (37%) (VWR, Rosny-sous-Bois, France). Perchloric acid ($HClO_4$) (60%), sodium hydroxide (NaOH) (98%), and sodium chloride (NaCl) (pure)(LOBA Chimie Pvt Ltd., Mumbai, India). All chemicals were used without further purification. Solutions were prepared using ultrapure water (Millipore MilliQ, Merck SA, Darmstadt, Allemagne) with a resistivity of 18.2 MΩ.cm. The initial pH of the solutions was adjusted with NaOH and $HClO_4$.

2.2. Preparation of Sodium Decatungstate

The procedure described in the literature [35] was slightly modified. A boiling solution of sodium tungstate (Na_2WO_4, $2H_2O$) was mixed with boiling 1.0 M hydrochloric acid and the mixture was refluxed to give a green solution according to the following equation:

$$10Na_2WO_4 + 16H^+ \longrightarrow Na_4W_{10}O_{32} + 8H_2O + 16Na^+ \quad (1)$$

To the above solution, solid sodium chloride was added with stirring, then brought to a boil, and then quickly placed in an ice-water bath. This suspended solution was kept in a freezer overnight. After 24 h, the crude $NaCl/Na_4W_{10}O_{32}$ suspension solution was filtered and the recovered solid was dissolved in acetonitrile. Then, the acetonitrile solution was heated under reflux and filtered to remove the insoluble NaCl. Finally, the acetonitrile solution was carefully evaporated in a hot water bath to obtain the $Na_4W_{10}O_{32}$ photocatalyst.

2.3. Photoreactor

The irradiation was performed with six mercury vapor lamps with a total power of 36 W. The envelope of the lamp is made of a special doping glass that allows the emission of UVB-UVA radiation like that of sunlight. The system is equipped with an internal reflector to focus the radiation and a Pyrex reactor((Sigma Aldrich, Shanghai, China) located 10 cm from each lamp with a double envelope that allows constant circulation of water. This type of glass reactor cuts the wavelengths below 300 nm to avoid direct photolysis. The device is equipped with a magnetic stirrer to ensure the homogeneity of the solution.

2.4. Procedure

In total, 30 mL of the samples containing the SMZ (27.8 mg/L) and catalyst (0.5 g/L) was added to the reactor (UVA/UVB-36W). The lamps were then turned on to trigger a light response. Throughout the reaction, stirring and aeration were maintained to keep the suspension homogeneous.

2.5. Analysis

Spectrophotometric measurements were recorded using a UV-6300PC spectrophotometer equipped with UV-Vis Analyst software for storage and processing of spectra. Quartz cells with an optical path length of 1 cm were used. Intermediates formed during SMZ degradation were determined with high-performance liquid chromatography (HPLC) using a Shimadzu LC-2030C 3D (Shimadzu Corporate, Kyoto, Japan) plus with a UV-vis detector. This system is connected to a data acquisition and processing unit, which operates using the analysis software.

An EC 250/4,6 Nucleodur 100-5 C18ec (Thermo Fisher Scientific, Illkirch, France) column was used, and the analysis was performed with an isocratic method using a mobile phase of ultrapure water and acetonitrile (40/60, v/v). The flow rate was set at 0.8 mL/min, and the temperature was maintained at 30 °C. Under these conditions, SMZ retention time was 7.9 min and the detection wavelength was 264 nm.

Identification of photoproducts from the photocatalytic degradation of SMZ was performed using HPLC coupled with time-of-flight mass spectrometry (TOF-MS). The instrument used was a Q-tof-Micro/Water 2699 (Thermo Fisher Scientific, Illkirch, France). The mode used in this technique is "Positive Electrospray Ionization"/ESI^+. This is an ionization method that results in the formation of protonated molecules with m/z = $[M+ H]^+$. The scan was performed in the m/z range between 50 and 400.

2.6. Computational Details

Theoretical investigations were performed with DFT calculations using the Gaussian 09W program [36] to predict the photodegradation mechanism of SMZ. The geometry optimization of SMZ, intermediates, and products was performed with a B3LYP/6-311G(d,p) basis set [37,38] using water as a solvent with the conductor-like polarizable continuum solvent model [39]. Moreover, the Fukui functions were calculated to predict the most electrophilic and nucleophilic sites, explaining the highest possible photodegradation mechanism of SMZ in the presence of the decatungstate anion under UV irradiation in an aqueous medium [40].

3. Results

3.1. Characterization

The crystalline structure, surface morphology, and thermal stability of the decatungstate anion were thoroughly explored in our previous studies in perfect agreement with the literature [41]. The UV-vis absorption spectrum of decatungstate (Figure 1a) shows distinct bands in the UV region due to the ligand-to-metal charge transfer (LMCT) process: electrons are transferred from the oxygen ligand O^{2-} (2p) to the tungsten metal W^{+6} (5d). It shows an absorption band centered at 324 nm with a molar absorption coefficient of 14,700 ± 300 $M^{-1}.cm^{-1}$. This shows a remarkable overlap with the solar emission spectrum (Figure 1b). Indeed, its excitation in its lowest energy band, λ > 300 nm, seems to be the easiest irradiation to realize from the practical point of view for potential applications [31,41].

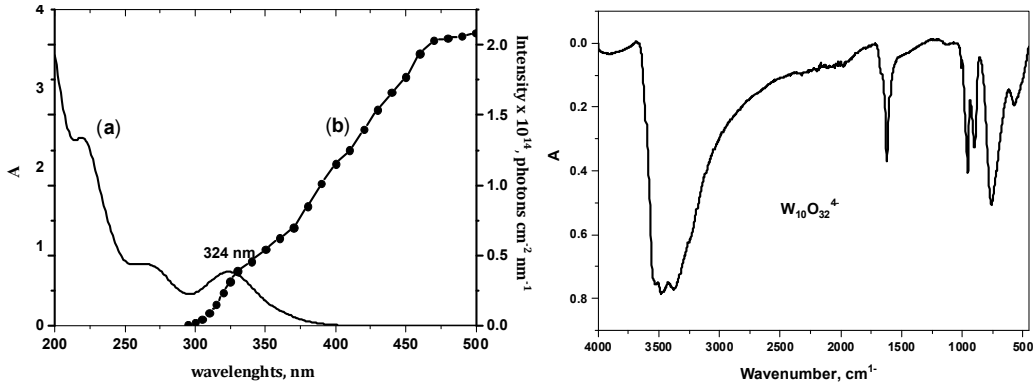

Figure 1. UV−vis spectrum of $W_{10}O_{32}{}^{4-}$ (0.27 g/L), pH = 4.5, in aqueous solution (a) and solar light emission (b) (**left**) and FTIR spectrum of $W_{10}O_{32}{}^{4-}$ (**right**).

The FT-IR spectrum of $W_{10}O_{32}{}^{4-}$ contains several bands with different positions and intensities. In particular, the strong band at 958 cm is characteristic of the stretching vibration of the W = O_t bond, while the vibration due to the deformation of the W-O_b-W bond is observed at about 889 to 768 cm (Figure 1) [27,42]. The broad band at 3400 cm^{-1} and the peak at 1620 cm^{-1} are also worth mentioning, which are due to the O-H stretching vibration and the bending modes of the water molecule.

3.2. Kinetics of SMZ Degradation

The SMZ UV absorption spectrum (Figure S1), recorded at 1.0 × 10^{-4} mol/L and pH = 4, shows two maximum wavelengths around 240 and 260 nm. Since absorption is

observed at λ > 295 nm, SMZ is therefore susceptible to direct degradation by sunlight. Therefore, the photodegradation of SMZ (27.8 mg/L, pH = 4) in an aqueous solution was followed both in the presence and absence of $W_{10}O_{32}^{4-}$ (0.5 g/L). The evolution of SMZ degradation as a function of irradiation time is presented in Figure 2.

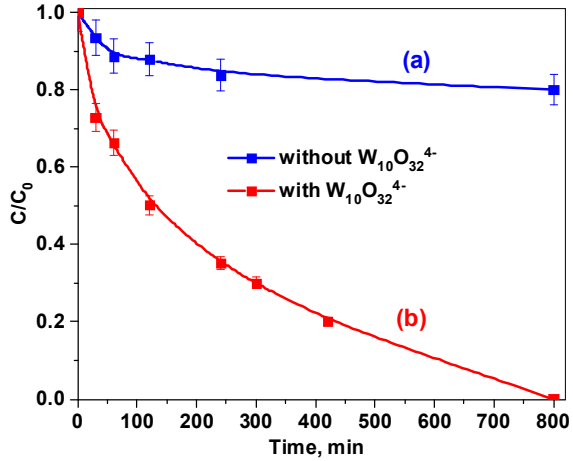

Figure 2. Kinetic study of an SMZ solution in the absence (a) and presence of decatungstate (b) ([SMZ] = 27.8 mg/L, $[W_{10}O_{32}^{4-}]$ = 0.5 g/L, pH=4, irradiation: UVA/UVB−36 W).

The results indicate that the presence of $Na_4W_{10}O_{32}$ allows the induced SMZ degradation by photocatalysis. In fact, in the absence of the photocatalyst, only a small percentage of degradation was observed upon direct light excitation, highlighting the quite good photochemical stability of SMZ under the experimental conditions. In contrast, the pollutant completely disappears in the presence of $W_{10}O_{32}^{4-}$ after 13 h of irradiation (Figure 2). This degradation process corresponds to apparent first-order kinetics with a rate constant of 6.14×10^{-3} min^{-1} and a half-life time of about 2 h.

3.3. Effect of pH

Even if decatungstate is known as a very reactive species, it is necessary to control the pH in an aqueous solution because another species like $H_2W_{12}O_{40}^{6-}$ or/and $W_7O_{24}^{6-}$, absorbing at lower wavelengths, can exist in acid and alkaline conditions, respectively [43,44]. Therefore, the influence of pH was investigated, and the results are shown in Figure 3. Hence, the pH has a significant effect on the degradation kinetics of SMZ in the presence of decatungstate anions. The maximum efficiency is observed in a pH range of 5–6, with a rate constant of around 8×10^{-3} min^{-1}, and it remains promising (above 6×10^{-3} min^{-1}) at a pH similar to that of WWTP conditions.

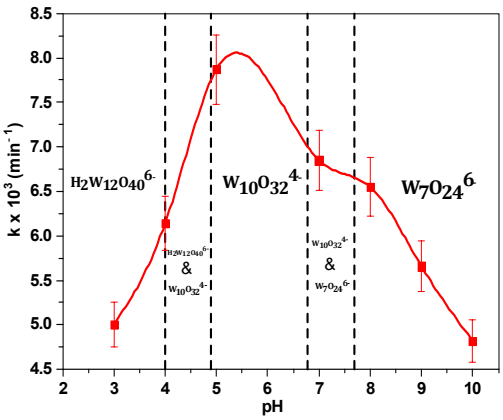

Figure 3. The evolution of the rate constant of SMZ degradation as a function of pH in the presence of decatungstate ([SMZ] =27.8 mg/L, $[W_{10}O_{32}^{4-}]$ =0.5 g/L, UVA/UVB−36W irradiation).

3.4. Pollutant Concentration Effect

The effect of SMZ concentration on the photocatalytic process was studied in the range of 2 to 83 mg/L with a constant photocatalyst dose (0.5 g/L) and pH (7). From the results shown in Figure 4, SMZ degradation decreases with increasing SMZ concentration. At the lower concentration (10^{-5} mol/L ≈ 2.78 ppm), SMZ disappears completely after 6 h of irradiation with a rate constant around 24 × 10^{-3} min^{-1} and a half-life time of 30 min. However, with the highest concentration, k and $t_{1/2}$ are 14 times lower and 16 times higher, respectively, and SMZ is partially eliminated (Table 1). This is probably due to a larger amount of SMZ to be degraded and to an absorbance competition between SMZ and the decatungstate anions, this being unfavorable for the photocatalytic reaction [17,45,46]. However, considering that the pollutant concentration under real natural conditions ranges from a few nanograms/liter to µg/L, it is reasonable to assume that this photocatalytic process could achieve complete degradation of SMZ and possibly its mineralization [47–49].

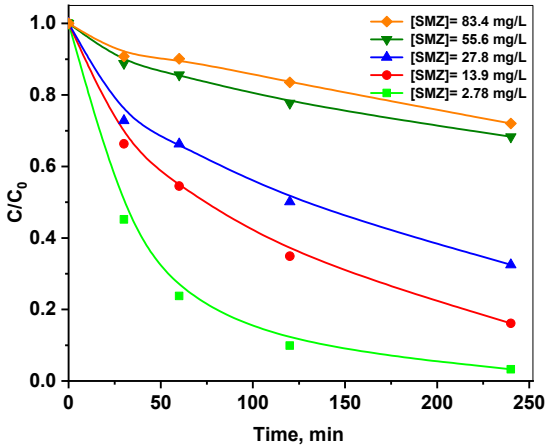

Figure 4. Photocatalytic degradation kinetics as a function of SMZ concentration ([$W_{10}O_{32}^{4-}$] = 0.5g/L, pH =7, irradiation: UVA/UVB-36 W).

Table 1. Initial rate constants and half-life times of photocatalytic degradation as a function of SMZ.

SMZ (mg/L)	2.78	13.9	27.8	55.6	83.4
$t_{1/2}$ (min)	30.2	66.1	101.2	267.6	471.5
k × 10^3 (min^{-1})	23.9	10.5	6.8	2.6	1.7

3.5. Decatungstate Mass Effect

To determine the optimal dose of the photocatalyst ($W_{10}O_{32}^{4-}$), a solution containing 13.9 mg/L of SMZ was maintained at a constant pH (7), and various masses of $Na_4W_{10}O_{32}$ were added to achieve concentrations of 0.16, 0.33, 0.5, and 0.66 g/L. Based on the determined initial rate constants (Figure 5), it was found that increasing the mass of the photocatalyst leads to an improvement in SMZ degradation until a plateau is reached for an optimal mass of 10 mg (equivalent to 0.33 g/L) (Figure 5). This is attributed to the potential aggregation of the photocatalyst at very high concentrations, which can lead to the formation of clumps. This, in turn, can reduce the surface area available for reactions and reduce the overall efficiency of the process [18,50–52].

A few studies focused on the elimination of other PP in water using decatungstate anions both in homogeneous and heterogeneous photocatalysis (Table 2). Hence, it was demonstrated that in homogeneous conditions, the degradation of PP is efficient depending on PP initial concentration, photocatalyst mass, and irradiation set up. In heterogeneous conditions, good results in the elimination of PP were also obtained, underlining the advancements and efficiencies of the decatungstate anion in pharmaceutical pollutant degradation [32,41,53].

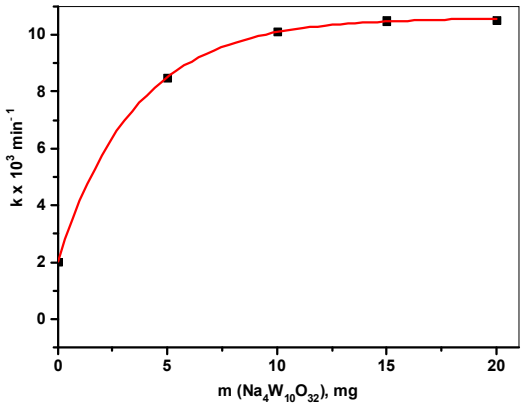

Figure 5. Evolution of the initial photocatalytic degradation rate of SMZ as a function of $Na_4W_{10}O_{32}$ mass ([SMZ] =13.9 mg/L, pH = 7, UVA/UVB−36 W irradiation).

Table 2. Comparison of photocatalytic efficiency for DCT across different Pollutants.

PP	Photocatalyst	Photocatalyst Mass (g/L)	PP (mg/L)	% Degradation	Time (h)	References
Sulfamethoxazole	$Na_4W_{10}O_{32}$	0.48	10	60	1	[53]
Propranolol	silica-$NH_3^+/Na_3W_{10}O_{32}^-$	5	10	60–65	3	[53]
Sulfasalazine	$Na_4W_{10}O_{32}$	0.097	19	16	2	[32]
Carbamazepine	$(CTAB)_4W_{10}O_{32}$	0.6	2.5	88.64	7	[41]
Carbamazepine	$Na_4W_{10}O_{32}$	0.6	2.5	45.64	7	[41]
Sulfamethazine	$Na_4W_{10}O_{32}$	0.33	13.9	85	4	This study

3.6. Effect of Oxygen Concentration

To understand the role of oxygen in SMZ-induced degradation, oxygen was removed using nitrogen bubbling before and during irradiation. The results shown in Figure 6 indicate that the degradation of SMZ in the presence of decatungstate is lower under deaerated conditions ($k = 1.1 \times 10^{-3}$ min^{-1}, $t_{1/2}$= 10.5 h) than under aerated conditions ($k = 10.11 \times 10^{-3}$ min^{-1}, $t_{1/2}$ = 1.8 h). This implies that oxygen is a key element in SMZ elimination. Namely, it enables the regeneration of $W_{10}O_{32}^{4-}$ from $W_{10}O_{32}^{5-}$, as shown in Equation (2) [25], with the continuous formation of reactive species. Such a photocatalytic cycle should favor the complete disappearance of SMZ in the solution.

$$W_{10}O_{32}^{5-} + O_2 \longrightarrow W_{10}O_{32}^{4-} + O_2^{\bullet -}, \quad (2)$$

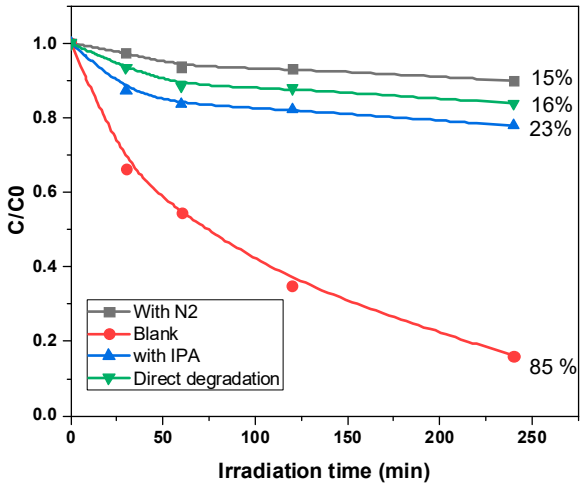

Figure 6. Photocatalytic degradation of SMZ in the presence of IPA and nitrogen ([SMZ] = 13.9 mg/L, pH = 7, $[Na_4W_{10}O_{32}]$ = 0.33 g/L, UVA/UVB-36 W irradiation).

3.7. Inhibition of Radical's Activity

It is well known that the species involved in the photocatalytic oxidation reactions are usually the photogenerated radicals ($HO^{\bullet}$). To study their contribution to this photocatalytic process, a solution of SMZ was irradiated in the presence of decatungstate, adding small amounts (2% v/v) of IPA. This alcohol was described as the most effective inhibitor of $HO^{\bullet}$, with a rate constant of 1.9×10^9 $M^{-1}.s^{-1}$ [46]. The inhibition reaction proceeds according to Equation (3):

$$(CH_3)_2CH\text{-}OH + {}^{\bullet}OH \longrightarrow (CH_3)_2C^{\bullet}\text{-}OH + H_2O \quad (3)$$

Figure 6 shows that the presence of IPA significantly slows down the photocatalytic degradation of SMZ (as well as the initial rate constant (Table 3)), but it remains higher than that in the absence of POM. This result indicates that hydroxyl radicals are mainly (about 81%) involved in the degradation of SMZ, and other radicals or reactive species are implicated in the process to a lesser extent.

Table 3. Rate constants of SMZ direct and photocatalytic degradation.

Conditions	$k \times 10^3$ (min^{-1})
Direct radiation	1.4
With 2% of IPA	1.9
Without IPA	10.1

3.8. Mineralization

Total degradation of a pollutant results in the conversion of organic carbon to harmless gaseous CO_2, while nitrogen and sulfur heteroatoms are converted to inorganic ions such as nitrate, ammonium, and sulfate ions, respectively. Figure 7 illustrates the mineralization profiles of SMZ at an initial concentration of 13.9 mg/L (equivalent to 7.2 mgC/L) in the presence of decatungstate anion photocatalysts at 0.33 g/L under UV-vis irradiation at a pH of 7. From Figure 7, it can be seen that the total organic carbon content decreases significantly upon irradiation without an induction period, and SMZ is completely converted into carbon dioxide in almost 100 h.

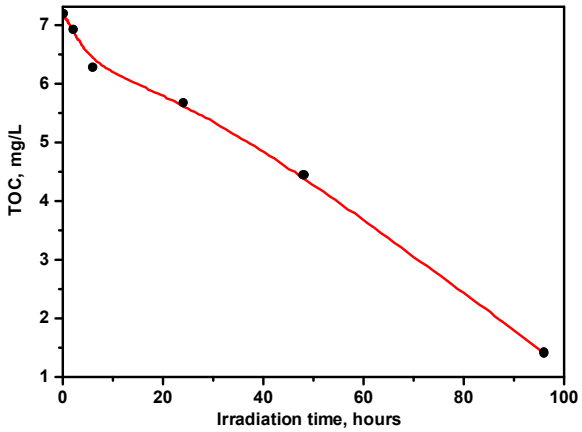

Figure 7. Photocatalytic mineralization of SMZ by decatungstate anion ([SMZ] =13.9 mg/L, $[Na_4W_{10}O_{32}]$ = 0.33 g/L, pH = 7, UVA/UVB-36 W irradiation).

3.9. LC-MS Studies for Product Analysis

The irradiated solutions were analyzed with liquid chromatography coupled to electrospray time-of-flight mass spectrometry (LC–ESI+TOF–MS) in the positive mode. The chromatogram shown in Figure 8. is the one of a solution of SMZ irradiated 30 min in the presence of the decatungstate anion ([SMZ] = 13.9 mg/L; $[W_{10}O_{32}{}^{4-}]$ = 0.33 g/L, pH = 7) with a conversion level of 30%.

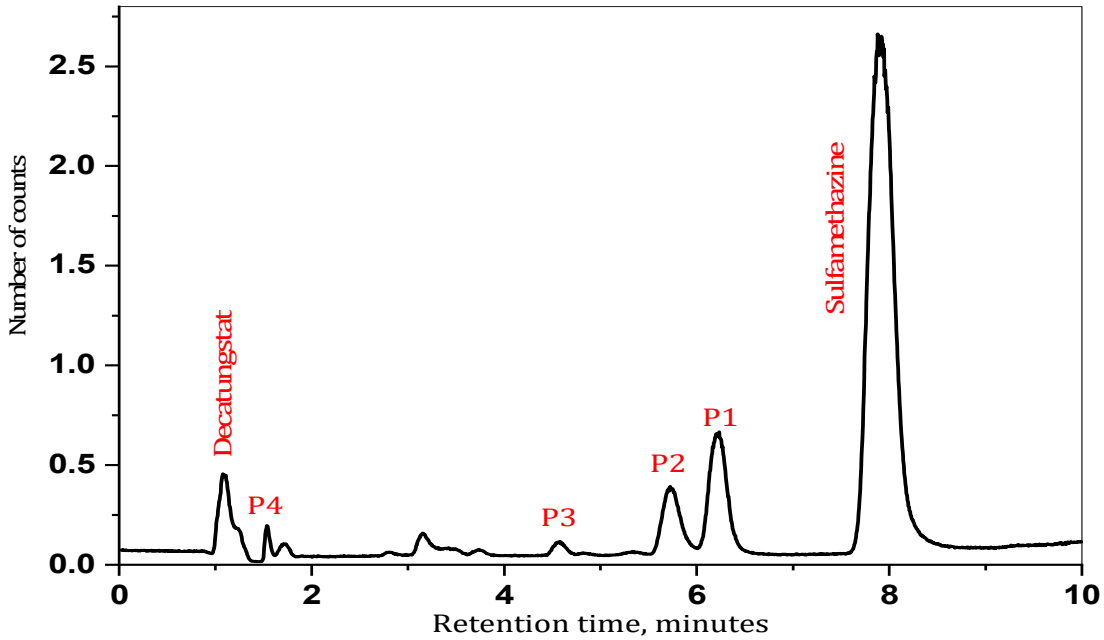

Figure 8. HPLC/TIC chromatogram of a solution of SMZ (13.9 mg/L) irradiated for 30 min in the presence of photocatalyst $W_{10}O_{32}^{4-}$ (0.33 g/L) at pH = 7.

Under our experimental conditions, several photoproducts (P1-P4) were formed with a shorter retention time compared to the starting product (SMZ, t_r = 7.88 min). This is in complete agreement with the formation of more polar and/or smaller molecules. All the results obtained are listed in Table 4.

Supplementary experiments with different collision energies (CEs) were performed to obtain more and irrefutable information about the hypothetical and unknown structure of the transformation products. After isolation and fragmentation of the precursor ion, the mass spectra obtained at different CE (10, 20, and 30 eV) were also complied in the Supporting Information.

SMZ was eluted after about 7.9 min and its ESI^+ mass spectrum (Figure S2) shows, among others, two peaks at m/z 279 (100%) and 301 (1.9%) corresponding to $[SMZ+H]^+$ and $[SMZ+Na]^+$, respectively. Moreover, in agreement with the literature [10,54–56], several peaks are observed at m/z 204, 186, 156, 124, 108, and 92, corresponding to fragments formed by the scission of the C-S and S-N bonds.

The photoproducts P1 and P2 were formed as primary products because they were readily observed during the first hours of irradiation. These two compounds are isomers since they have the same m/z = 295, with retention times of 6.25 and 5.7 min, respectively (Table 4). Considering their mass difference with SMZ (16 Da), both products should correspond to hydroxylated SMZ derivatives.

The Collision-Induced Dissociation (CID) spectrum of P1 shows three common product ions with SMZ at 204, 186, and 124 (Figure S3), indicating that the OH group is not located on the pyrimidine moiety. This is confirmed with the two fragment ions (m/z =186 and 124) indicating the addition of 16 Da to the observed SMZ fragments (m/z =172 and 108) corresponding to the aromatic moiety. This suggests that the hydroxyl group in compound P1 is located on the aromatic moiety [57]. However, the precise position of the OH group remains unknown.

Similarly, comparison of the mass spectra of P2 and SMZ CID (Figure S4) reveals the presence of three common ions containing the aromatic cycle (108, 156, and 92), while all other fragment ions containing the pyrimidine moiety indicate the addition of 16 Da. This indicates the presence of an OH-function in the free para position of the pyrimidine moiety [54,55,57].

Table 4. Retention time (tr), ratio of mass/charge (m/z), elementary formula of protonated compound $[M+ H]^+$, mass difference with SMZ (ΔM), and proposed chemical structures of SMZ photoproducts, analyzed with the LC/MS/ESI$^+$.

t_r (min)	Products	m/z	Formula	ΔM	Chemical Structure
7.88	SMZ	279	$C_{12}H_{15}N_4O_2S$		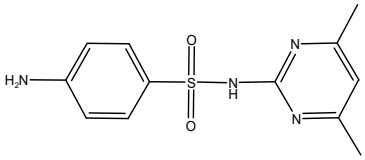
6.25	P1	295	$C_{12}H_{15}N_4O_3S$	+16	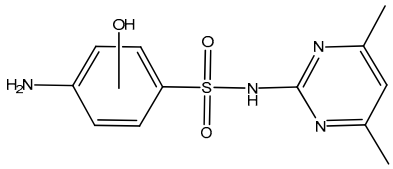
5.74	P2	295	$C_{12}H_{15}N_4O_3S$	+16	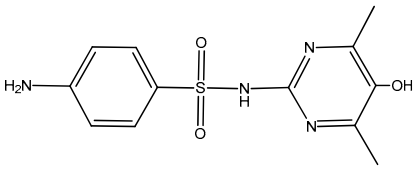
4.57	P3	311	$C_{12}H_{15}N_4O_4S$	+32	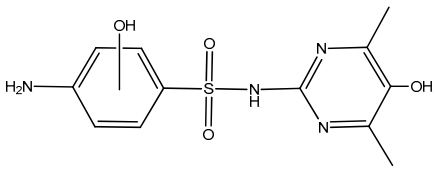
1.70	P4	215	$C_{12}H_{15}N_4$	−64	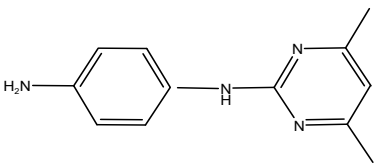

Compound P3 has a mass difference of 32 Da compared with SMZ, indicating the presence of 2 OH functions (Table 4). From Figure S5, the fragments at m/z 124, 172, and 245 confirm the presence of an OH group on the aromatic ring and the ones at m/z 140 and 202 confirm the presence of the same group on the pyrimidine moiety. Compound P3 corresponds to SMZ substituted by two OH functions, one on the aromatic ring and the other on the pyrimidine moiety, without information on the OH position on the benzene [57].

The CID spectrum of P4 shows a fragment ion at m/z = 215, which is due to a mass loss of 34 Da from SMZ that could be attributed to the loss of the SO_2 group (Table 4). This is confirmed by the absence of the $[M + H + 2]^+$ fragment at m/z = 217, which is characteristic of the ^{34}S isotope (Figure S6). Moreover, the presence of the two fragments at m/z = 124 and 92, corresponding to the aromatic and pyrimidine moieties, respectively, confirms the proposed structure of P4.

3.10. Mechanism of Photocatalytic Degradation of SMZ

The photocatalytic degradation pathways of SMZ by decatungstate anions under light irradiation have been elucidated with previous results and DFT calculations [58]. Fukui indices representing the most electrophilic (f_k^-) and radical attack (f^0) sites of atoms on the SMZ molecule are shown in Figure 9 [59–62].

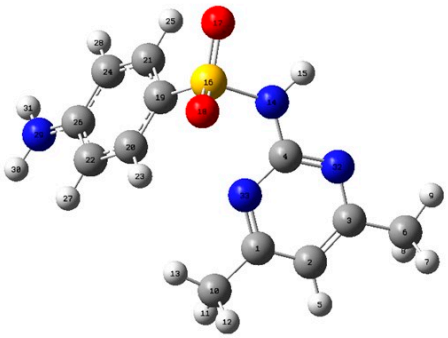

SMZ

Atome	Num	Electrophilic Attack (f^-)	f^0
C	1	0.00865	0.013775
C	2	0.10938	0.066185
C	3	0.00527	0.01918
C	4	-0.00285	0.002605
C	6	-0.00251	-0.00342
C	10	-0.00207	-0.002125
N	14	0.05599	0.040165
S	16	-0.01536	0.01802
O	17	0.03693	0.042735
O	18	0.0427	0.046605
C	19	0.04975	0.034285
C	20	-0.00712	0.032255
C	21	**0.14471**	**0.109715**
C	22	0.01149	0.075695
C	24	0.10441	0.055235
C	26	-0.0011	0.061725
N	29	0.20886	0.13631
N	32	0.03325	0.02406
N	33	0.01815	0.01663

Figure 9. Chemical structure and Fukui functions (f^- f^0) of SMZ.

The Fukui functions show that carbon atoms C21 and C22 of the aromatic ring and C2 of the pyrimidine moiety are the most reactive sites, which is confirmed by the highest value of f^0 and f^- (Figure 9). This indicates that these sites are the hydroxylation sites corresponding to P1, P2, and P3 photoproducts. In addition, the energetic barriers for the hydroxylation step were calculated using the DFT calculation via the B3LYP/6−311G(d,p) basis set with water as the solvent. The energetic barrier for the formation of the hydroxylated product P1 is 19.57 kcal/mol and for P3, it is 11.20 kcal/mol. These results confirm that the most favorable product is P3 as reported by Xu et al. [63].

Accordingly, it can be suggested that the initial steps of SMZ degradation occur with the direct addition of the hydroxyl group to carbon C2 of the pyrimidine group (most favorable) and to a lesser extent to carbon C21 and C22 of the aromatic ring (Scheme 1).

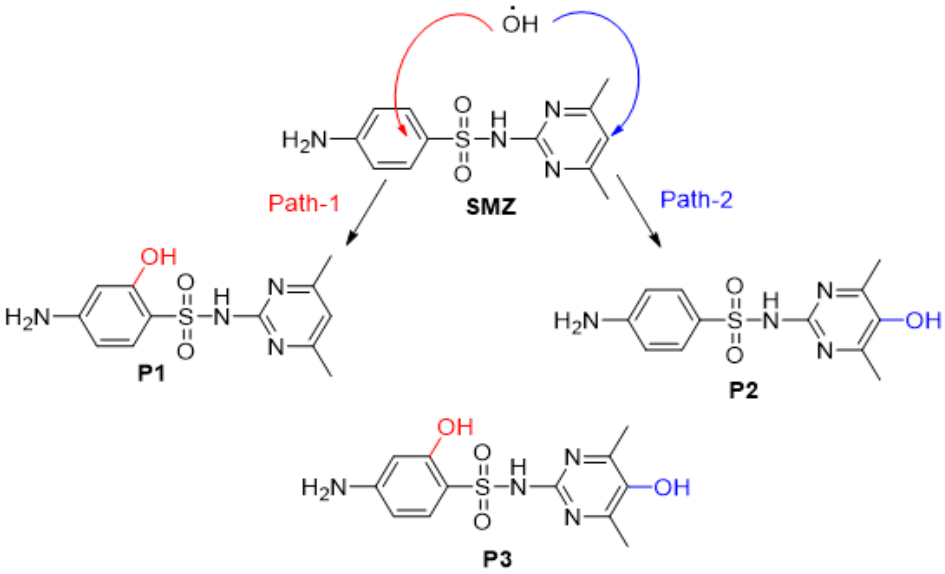

Scheme 1. Formation mechanism of hydroxylated photoproducts (P1, P2, and P3) generated by the photocatalytic degradation of SMZ.

However, as we demonstrated that SMZ transformation could occur in the presence of a hydroxyl radical quencher, one can suppose the involvement of another mechanism. In fact, the photoproducts can also be formed with an electron transfer from the aromatic and pyrimidine groups to $W_{10}O_{32}^{4-*}$ (redox process) followed by the addition of oxygen (pathway 3 and 4) (Scheme 2).

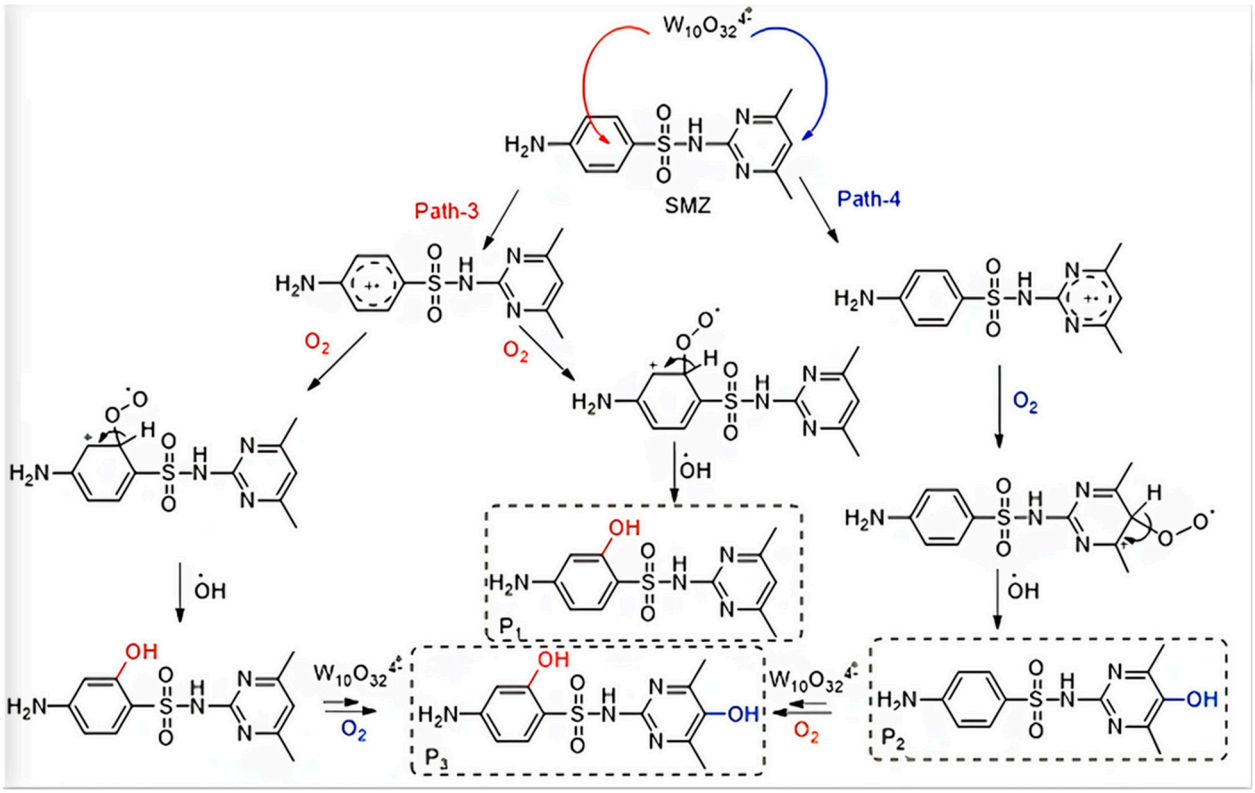

Scheme 2. Formation mechanism of hydroxylated photoproducts (P1, P2, and P3) generated by the photocatalytic degradation of SMZ.

In addition, the analysis of the Fukui functions shows that the sulfur atom has a significative value of f^0, confirming the possibility of radical attack at this molecular site (see Figure 9). This suggests that the desulfurization reaction can be carried out with the attack of the hydroxyl radical on the sulfur atom. Such a reaction was recently described by Cheng et al. [32] with the attack of the hydroxyl radical on the adjacent amine group via an electron or/and a hydrogen abstraction process. The desulfurization reaction leads to the formation of two radicals, whose recombination (in-cage rearrangement) can lead to compound P4 (Scheme 3). Since the energetic barrier for the formation of the byproduct P4 is 2.52 kcal/mol, this confirms its favorable formation.

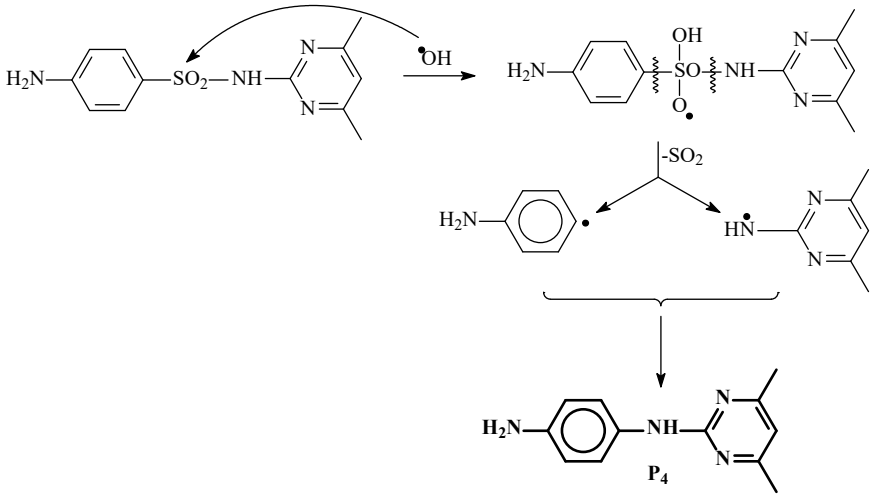

Scheme 3. Formation mechanism of the photoproduct P4 obtained by the photocatalytic degradation of SMZ.

4. Conclusions

In this work, the decatungstate anion has shown very high photocatalytic activity under UVA and UVB light excitation in the degradation of SMZ in water. The process requires the presence of oxygen, as a key element in the photocatalytic cycle, and is optimized in the pH range of 5-6 with a decatungstate mass concentration of 0.33 g/L in the presence of 13.9 mg/L of SMZ. Hydroxyl radicals are mainly involved in SMZ elimination and are continuously generated during the irradiation of the decatungstate anion in water, allowing SMZ mineralization. SMZ elimination occurs mainly through the cleavage of the sulphonamide bridge, and by the hydroxylation of both the aromatic ring and the pyrimidine group to a lesser extent.

Supplementary Materials: The following supporting information can be downloaded at: https://www.mdpi.com/article/10.3390/w15234058/s1. Figure S1: Molecular structure of SMZ. Figure S2: Absorption spectrum of the Sulfamethazine ([SMZ] =27.8 mg/L, pH=4 in water), Figure S3: CID spectrum of SMZ (CE = 20 eV), Figure S4: CID spectrum of P1 (CE = 20 eV), Figure S5: CID spectrum of P2 (CE = 20 eV), Figure S6: CID spectrum of P3 (CE = 20 eV), Figure S7: CID spectrum of P4 (CE = 20 eV)

Author Contributions: Conceptualization, S.R.; Methodology, Investigation, Visualization, Data curation, Writing—original draft, M.-A.E. and L.E.M.; Writing—original draft preparation, M.-A.E.; Writing—review and editing, S.R., P.W.-W.-C., L.E.B., M.M.A. and A.A.T.; Supervision, S.R. and A.A.T.; Project administration, Funding acquisition, L.E.B., M.M.A. and S.R. All authors have read and agreed to the published version of the manuscript.

Funding: This research was funded by the Researchers Supporting Project (number RSPD2023R774), King Saud University, Riyadh, Saudi Arabia.

Data Availability Statement: Data available on request due to restrictions eg privacy or ethical.

Acknowledgments: The authors gratefully acknowledge EL MOUCHTARI El Mountassir and BAHSIS Lahoucine for their collaboration and King Saud University (Riyadh, Saudi Arabia) for its financial support (Researchers Supporting Project, number RSPD2023R774).

Conflicts of Interest: The authors declare no conflict of interest.

References

1. Fatta-Kassinos, D.; Hapeshi, E.; Achilleos, A.; Meric, S.; Gros, M.; Petrovic, M.; Barcelo, D. Existence of Pharmaceutical Compounds in Tertiary Treated Urban Wastewater That Is Utilized for Reuse Applications. *Water Resour. Manag.* **2011**, *25*, 1183–1193. [CrossRef]
2. El-Dairi, M.; House, R.J. Veterinary Drugs in the Environment and Their Toxicity to Plants. In *Handbook of Pediatric Retinal OCT and the Eye-Brain Connection*; Elsevier: Amsterdam, The Netherlands, 2020; pp. 285–287. [CrossRef]
3. Girard, P. Toxiques et Poisons Dans Le Passé Pharmaceutique de La Savoie. *Rev. D'histoire Pharm.* **1983**, *71*, 287–297. [CrossRef]
4. An, T.; Yang, H.; Song, W.; Li, G.; Luo, H.; Cooper, W.J. Mechanistic Considerations for the Advanced Oxidation Treatment of Fluoroquinolone Pharmaceutical Compounds Using TiO_2 Heterogeneous Catalysis. *J. Phys. Chem. A* **2010**, *114*, 2569–2575. [CrossRef] [PubMed]
5. Ray, M.B. Photocatalytic Oxidation of Paracetamol: Dominant Reactants, Intermediates, and Reaction Mechanisms. *Environ. Sci. Technol.* **2009**, *43*, 460–465.
6. Xu, W.; Zhang, G.; Zou, S.; Li, X.; Liu, Y. Determination of Selected Antibiotics in the Victoria Harbour and the Pearl River, South China Using High-Performance Liquid Chromatography-Electrospray Ionization Tandem Mass Spectrometry. *Environ. Pollut.* **2007**, *145*, 672–679. [CrossRef]
7. Connor, E.E. Sulfonamide Antibiotics. *Prim. Care Update OB/GYNS* **1998**, *5*, 32–35. [CrossRef]
8. García-Galán, M.J.; Díaz-Cruz, M.S.; Barceló, D. Occurrence of Sulfonamide Residues along the Ebro River Basin. Removal in Wastewater Treatment Plants and Environmental Impact Assessment. *Environ. Int.* **2011**, *37*, 462–473. [CrossRef]
9. Göbel, A.; McArdell, C.S.; Suter, M.J.F.; Giger, W. Trace Determination of Macrolide and Sulfonamide Antimicrobials, a Human Sulfonamide Metabolite, and Trimethoprim in Wastewater Using Liquid Chromatography Coupled to Electrospray Tandem Mass Spectrometry. *Anal. Chem.* **2004**, *76*, 4756–4764. [CrossRef]
10. García-Galán, M.J.; Díaz-Cruz, M.S.; Barceló, D. Kinetic Studies and Characterization of Photolytic Products of Sulfamethazine, Sulfapyridine and Their Acetylated Metabolites in Water under Simulated Solar Irradiation. *Water Res.* **2012**, *46*, 711–722. [CrossRef]

11. García-Galán, M.J.; Frömel, T.; Müller, J.; Peschka, M.; Knepper, T.; Díaz-Cruz, S.; Barceló, D. Biodegradation Studies of N^4-Acetylsulfapyridine and N^4-Acetylsulfamethazine in Environmental Water by Applying Mass Spectrometry Techniques. *Anal. Bioanal. Chem.* **2012**, *402*, 2885–2896. [CrossRef]
12. Padmaja, K.; Cherukuri, J.; Anji Reddy, M. A Comparative Study of the Efficiency of Chemical Coagulation and Electrocoagulation Methods in the Treatment of Pharmaceutical Effluent. *J. Water Process. Eng.* **2020**, *34*, 101153. [CrossRef]
13. Naboulsi, A.; Naboulsi, I.; Bouzid, T.; Grich, A.; Regti, A.; El Himri, M.; El Haddad, M. Tetracycline Removal by a Natural Biosorbent: Optimization by Response Surface Methods Employing DOE/FFD Design of the Experiment. *Int. J. Environ. Anal. Chem.* **2023**, *103*, 1–22. [CrossRef]
14. Joss, A.; Keller, E.; Alder, A.C.; Go, A.; Mcardell, C.S.; Ternes, T.; Siegrist, H. Removal of Pharmaceuticals and Fragrances in Biological Wastewater Treatment. *Water Res.* **2005**, *39*, 3139–3152. [CrossRef]
15. Ataklti, A.; Alemu, K.; Abebe, B. Study of the Self-Association of Amoxicillin, Thiamine and the Hetero-Association with Biologically Active Compound Chlorgenic Acid. *Afr. J. Pharm. Pharmacol.* **2016**, *10*, 393–402. [CrossRef]
16. Rai, B.; Shrivastav, A. Removal of Emerging Contaminants in Water Treatment by Nanofiltration and Reverse Osmosis. In *Development in Wastewater Treatment Research and Processes: Removal of Emerging Contaminants from Wastewater through Bio-Nanotechnology*; Elsevier: Amsterdam, The Netherlands, 2022; pp. 605–628. [CrossRef]
17. Lekbira, E.M.; El Mouchtari, E.; Belghiti, M.; Belkodia, K.; Edaala, M.A.; Briche, S.; Tahiri, A.A.; Rafqah, S. Development of a New Composite LDH/TiO_2-3D for Degradation of Sulfaguanidine under UV and Visible Light: Experimental Design, Kinetic and Mechanisms. *J. Environ. Chem. Eng.* **2023**, 111038. [CrossRef]
18. Belghiti, M.; El Mersly, L.; El Mouchtari, E.M.; Rafqah, S.; Ouzaouit, K.; Faqir, H.; Benzakour, I.; Oueriagli, A.; Outzourhit, A. Synthesis and Characterization of Y_2O_3 Partially Coated ZnO for Highly Efficient Photocatalytic Degradation of Sulfamethazine. *J. Mol. Struct.* **2022**, *1251*, 132036. [CrossRef]
19. El Mouchtari, E.M.; El Mersly, L.; Belkodia, K.; Piram, A.; Lebarillier, S.; Briche, S.; Rafqah, S.; Wong-Wah-Chung, P. Sol-Gel Synthesis of New TiO_2 Ball/Activated Carbon Photocatalyst and Its Application for Degradation of Three Hormones: 17α-EthinylEstradiol, Estrone, and β-Estradiol. *Toxics* **2023**, *11*, 299. [CrossRef] [PubMed]
20. El Mouchtari, E.M.; El Mersly, L.; Jhabli, O.; Anane, H.; Piram, A.; Briche, S.; Wong-Wah-Chung, P.; Rafqah, S. Hydrothermal Synthesis of 3D Cauliflower Anatase TiO_2 and Bio Sourced Activated Carbon: Adsorption and Photocatalytic Activity in Real Water Matrices. *Int. J. Environ. Anal. Chem.* **2022**, *102*, 1–16. [CrossRef]
21. Umar, A.; Kumar, R.; Kumar, G.; Algarni, H.; Kim, S.H. Effect on Annealing Temperature on the Properties and Photocatalytic Efficiencies of ZnO Nanoparticles. *J. Alloys Compd.* **2015**, *648*, 46–52. [CrossRef]
22. Sood, S.; Kumar, S.; Umar, P.A.; Kaur, A.; Mehta, S.K.; Sushil, P.; Kansal, K. TiO_2 Quantum Dots for the Photocatalytic Degradation of Indigo Carmine Dye. *J. Alloys Compd.* **2015**, *650*, 193–198. [CrossRef]
23. Tanielian, C. Decatungstate Photocatalysis. *Coord. Chem. Rev.* **1998**, *178–180*, 1165–1181. [CrossRef]
24. Suzuki, K.; Mizuno, N.; Yamaguchi, K. Polyoxometalate Photocatalysis for Liquid-Phase Selective Organic Functional Group Transformations. *ACS Catal.* **2018**, *8*, 10809–10825. [CrossRef]
25. Choina, J.; Kosslick, H.; Fischer, C.; Flechsig, G.U.; Frunza, L.; Schulz, A. Photocatalytic Decomposition of Pharmaceutical Ibuprofen Pollutions in Water over Titania Catalyst. *Appl Catal B* **2013**, *129*, 589–598. [CrossRef]
26. Li, C.; Gu, C.; Yamaguchi, K.; Suzuki, K. Highly Efficient Degradation of Polyesters and Polyethers by Decatungstate Photocatalysis. *Nanoscale* **2023**, *15*, 15038–15042. [CrossRef]
27. Stiriba, S.E.; Aflak, N.; El Mouchtari, E.M.; Ben El Ayouchia, H.; Rafqah, S.; Anane, H.; Julve, M. Merging Decatungstate Photocatalysis and Copper-Catalyzed Azide-Alkyne Cycloaddition Reaction for the Formation of 1,2,3-Triazoles in Water†. *Appl. Organomet. Chem.* **2023**, *37*, e7175. [CrossRef]
28. Mylonas, A.; Papaconstantinou, E. Photocatalytic Degradation of Chlorophenols to CO_2 and HCl with Polyoxotungstates in Aqueous Solution. *J. Mol. Catal.* **1994**, *92*, 261–267. [CrossRef]
29. Mylonas, A.; Papaconstantinou, E. On the Mechanism of Photocatalytic Degradation of Chlorinated Phenols to CO_2 and HCl by Polyoxometalates. *J. Photochem. Photobiol. A Chem.* **1996**, *94*, 77–82. [CrossRef]
30. Texier, I.; Giannotti, C.; Malato, S.; Richter, C.; Delaire, J. Solar Photodegradation of Pesticides in Water by Sodium Decatungstate. *Catal. Today* **1999**, *54*, 297–307. [CrossRef]
31. Tanielian, C.; Lykakis, I.N.; Seghrouchni, R.; Cougnon, F.; Orfanopoulos, M. Mechanism of Decatungstate Photocatalyzed Oxygenation of Aromatic Alcohols: Part I. Continuous Photolysis and Laser Flash Photolysis Studies. *J. Mol. Catal. A Chem.* **2007**, *262*, 170–175. [CrossRef]
32. Loaiza-Ambuludi, S.; Panizza, M.; Oturan, N.; Oturan, M.A. Removal of the Anti-Inflammatory Drug Ibuprofen from Water Using Homogeneous Photocatalysis. *Catal Today* **2014**, *224*, 29–33. [CrossRef]
33. Sudan Amoksisilin, A.; Ampisillin, V.E.; Giderimi, A. Amoxicillin and Ampicillin Removal from Wastewater by Fenton and Photo-Fenton Processes Fenton Ve Foto-Fenton Prosesleri Kullanarak. Ph.D. Thesis, Hacettepe University, Ankara, Turkey, 2015.
34. Fukahori, S.; Fujiwara, T. Photocatalytic Decomposition Behavior and Reaction Pathway of Sulfamethazine Antibiotic Using TiO_2. *J. Environ. Manag.* **2015**, *157*, 103–110. [CrossRef]
35. Cheng, P.; Wang, Y.; Sarakha, M.; Mailhot, G. Enhancement of the Photocatalytic Activity of Decatungstate, W10O324−, for the Oxidation of Sulfasalazine/Sulfapyridine in the Presence of Hydrogen Peroxide. *J. Photochem. Photobiol. A Chem.* **2021**, *404*, 112890. [CrossRef]

36. Frisch, M.J.; Trucks, G.W.; Schlegel, H.B.; Scuseria, G.E.; Robb, M.A.; Cheeseman, J.R.; Scalmani, G.; Barone, V.; Mennucci, B.; Petersson, G.A.; et al. *Gaussian 09*; Gaussian Inc.: Wallingford, CT, USA, 2009.
37. Becke, A.D. Density-functional Thermochemistry. III. The Role of Exact Exchange. *J. Chem. Phys.* **1993**, *98*, 5648–5652. [CrossRef]
38. Lee, C.; Yang, W.; Parr, R.G. Development of the Colle-Salvetti Correlation-Energy Formula into a Functional of the Electron Density. *Phys. Rev. B* **1988**, *37*, 785–789. [CrossRef]
39. Tomasi, J.; Persico, M. Molecular Interactions in Solution: An Overview of Methods Based on Continuous Distributions of the Solvent. *Chem. Rev.* **1994**, *94*, 2027–2094. [CrossRef]
40. Ayers, P.W.; Parr, R.G. Variational Principles for Describing Chemical Reactions: The Fukui Function and Chemical Hardness Revisited. *J. Am. Chem. Soc.* **2000**, *122*, 2010–2018. [CrossRef]
41. Briche, S.; El Mouchtari, E.M.; Boutamart, M.; Jhabli, O.; EL Mersly, L.; Belkodia, K.; Edaala, M.A.; Wong-Wah-Chung, P.; Abida, O.; Rafqah, S. Synthesis and Characterization of New Hybrid Decatungstate Anions $(CTAB)_4W_{10}O_{32}$: Toward Heterogeneous Photocatalysis. *Int. J. Environ. Anal. Chem.* **2023**, 1–18. [CrossRef]
42. Renneke, R.F.; Pasquali, M.; Hill, C.L. Polyoxometalate Systems for the Catalytic Selective Production of Nonthermodynamic Alkenes from Alkanes. Nature of Excited-State Deactivation Processes and Control of Subsequent Thermal Processes in Polyoxometalate Photoredox Chemistry. *J. Am. Chem. Soc.* **1990**, *112*, 6585–6594. [CrossRef]
43. Errington, R.J.; Kerlogue, M.D.; Richards, D.G. Non-Aqueous Routes to a New Polyoxotungstate. *J. Chem. Soc. Chem. Commun.* **1993**, *7*, 649–651. [CrossRef]
44. Rafqah, S.; Chung, P.W.W.; Forano, C.; Sarakha, M. Photocatalytic Degradation of Metsulfuron Methyl in Aqueous Solution by Decatungstate Anions. *J. Photochem. Photobiol. A Chem.* **2008**, *199*, 297–302. [CrossRef]
45. Wang, C.; Ni, H.; Dai, J.; Liu, T.; Wu, Z.; Chen, X.; Dong, Z.; Qian, J.; Wu, Z. Comparison of Highly Active Type-I and Type-II Heterojunction Photocatalytic Composites Synthesized by Electrospinning for Humic Acid Degradation. *Chem. Phys. Lett.* **2022**, *803*, 139815. [CrossRef]
46. Mourid, E.H.; el Mouchtari, E.M.; el Mersly, L.; Benaziz, L.; Rafqah, S.; Lakraimi, M. Development of a New Recyclable Nanocomoposite LDH-TiO_2 for the Degradation of Antibiotic Sulfamethoxazole under UVA Radiation: An Approach towards Sunlight. *J. Photochem. Photobiol. A Chem.* **2020**, *396*, 112530. [CrossRef]
47. Larsson, D.G.J.; de Pedro, C.; Paxeus, N. Effluent from Drug Manufactures Contains Extremely High Levels of Pharmaceuticals. *J. Hazard Mater.* **2007**, *148*, 751–755. [CrossRef]
48. Carter, L.J.; Garman, C.D.; Ryan, J.; Dowle, A.; Bergström, E.; Thomas-Oates, J.; Boxall, A.B.A. Fate and Uptake of Pharmaceuticals in Soil-Earthworm Systems. *Environ. Sci. Technol.* **2014**, *48*, 5955–5963. [CrossRef]
49. Sim, W.J.; Lee, J.W.; Oh, J.E. Occurrence and Fate of Pharmaceuticals in Wastewater Treatment Plants and Rivers in Korea. *Environ. Pollut.* **2010**, *158*, 1938–1947. [CrossRef] [PubMed]
50. El Mouchtari, E.M.; Daou, C.; Rafqah, S.; Najjar, F.; Anane, H.; Piram, A.; Hamade, A.; Briche, S.; Wong-Wah-Chung, P. TiO_2 and Activated Carbon of Argania Spinosa Tree Nutshells Composites for the Adsorption Photocatalysis Removal of Pharmaceuticals from Aqueous Solution. *J. Photochem. Photobiol. A Chem.* **2020**, *388*, 112183. [CrossRef]
51. Thakur, R.S.; Chaudhary, R.; Singh, C. Fundamentals and Applications of the Photocatalytic Treatment for the Removal of Industrial Organic Pollutants and Effects of Operational Parameters: A Review. *J. Renew. Sustain. Energy* **2010**, *2*, 042701. [CrossRef]
52. Akpan, U.G.; Hameed, B.H. Parameters Affecting the Photocatalytic Degradation of Dyes Using TiO_2-Based Photocatalysts: A Review. *J. Hazard Mater.* **2009**, *170*, 520–529. [CrossRef]
53. Pasti, L.; Sarti, E.; Martucci, A.; Marchetti, N.; Stevanin, C.; Molinari, A. An Advanced Oxidation Process by Photoexcited Heterogeneous Sodium Decatungstate for the Degradation of Drugs Present in Aqueous Environment. *Appl. Catal. B* **2018**, *239*, 345–351. [CrossRef]
54. Gao, X.; Lu, J.; Ji, Y.; Chen, J.; Yin, X.; Zhou, Q. Nitrite-Mediated Photodegradation of Sulfonamides and Formation of Nitrated Products. *Chemosphere* **2021**, *282*, 130968. [CrossRef]
55. Oliveira, C.A.; Penteado, E.D.; Tomita, I.N.; Santos-Neto, Á.J.; Zaiat, M.; da Silva, B.F.; Lima Gomes, P.C.F. Removal Kinetics of Sulfamethazine and Its Transformation Products Formed during Treatment Using a Horizontal Flow-Anaerobic Immobilized Biomass Bioreactor. *J. Hazard Mater.* **2019**, *365*, 34–43. [CrossRef] [PubMed]
56. Kaniou, S.; Pitarakis, K.; Barlagianni, I.; Poulios, I. Photocatalytic Oxidation of Sulfamethazine. *Chemosphere* **2005**, *60*, 372–380. [CrossRef] [PubMed]
57. Briche, S.; Derqaoui, M.; Belaiche, M.; El Mouchtari, E.M.; Wong-Wah-Chung, P.; Rafqah, S. Nanocomposite Material from TiO_2 and Activated Carbon for the Removal of Pharmaceutical Product Sulfamethazine by Combined Adsorption/Photocatalysis in Aqueous Media. *Environ. Sci. Pollut. Res.* **2020**, *27*, 25523–25534. [CrossRef] [PubMed]
58. El Mouchtari, E.M.; Bahsis, L.; El Mersly, L.; Anane, H.; Lebarillier, S.; Piram, A.; Briche, S.; Wong-Wah-Chung, P.; Rafqah, S. Insights in the Aqueous and Adsorbed Photocatalytic Degradation of Carbamazepine by a Biosourced Composite: Kinetics, Mechanisms and DFT Calculations. *Int. J. Environ. Res.* **2021**, *15*, 135–147. [CrossRef]
59. Balasurya, S.; Okla, M.K.; Alaraidh, I.A.; Al-ghamdi, A.A.; Mohebaldin, A.; Abdel-Maksoud, M.A.; Abdelaziz, R.F.; Thomas, A.M.; Raju, L.L.; Khan, S.S. Sunlit Photocatalytic Degradation of Organic Pollutant by $NiCr_2O_4/Bi_2S_3/Cr_2S_3$ Tracheid Skeleton Nanocomposite: Mechanism, Pathway, Reactive Sites, Genotoxicity and Byproduct Toxicity Evaluation. *J. Environ. Manag.* **2022**, *319*, 115674. [CrossRef]

60. Okla, M.K.; Harini, G.; Dawoud, T.M.; Akshhayya, C.; Mohebaldin, A.; AL-ghamdi, A.A.; Soufan, W.; Abdel-Maksoud, M.A.; AbdElgawad, H.; Raju, L.L.; et al. Fabrication of $MnFe_2O_4$ Spheres Modified CeO_2 Nano-Flakes for Sustainable Photodegradation of MB Dye and Antimicrobial Activity: A Brief Computational Investigation on Reactive Sites and Degradation Pathway. *Colloids Surf. A Physicochem. Eng. Asp.* **2022**, *641*, 128566. [CrossRef]
61. Dabić, D.; Hanževački, M.; Škorić, I.; Žegura, B.; Ivanković, K.; Biošić, M.; Tolić, K.; Babić, S. Photodegradation, Toxicity and Density Functional Theory Study of Pharmaceutical Metoclopramide and Its Photoproducts. *Sci. Total Environ.* **2022**, *807*, 150694. [CrossRef]
62. Zhang, Q.; Chen, J.; Gao, X.; Che, H.; Ao, Y.; Wang, P. Understanding the Mechanism of Interfacial Interaction Enhancing Photodegradation Rate of Pollutants at Molecular Level: Intermolecular π-π Interactions Favor Electrons Delivery. *J. Hazard Mater.* **2022**, *430*, 128386. [CrossRef] [PubMed]
63. Yang, Z.; Sun, Y.; Hou, Z.; Yu, H.; Li, M.; Li, Y.; Li, Y.; Gao, B.; Xu, S. Repeated Fluctuation of Cu^{2+} Concentration during Photocatalytic Purification of SMZ-Cu^{2+} Combined Pollution: Behavior, Mechanism and Application. *J. Hazard Mater.* **2023**, *447*, 130768. [CrossRef] [PubMed]